



Proliferation inhibition of novel diphenylamine derivatives

Ladislav Janovec^{a,*}, Jana Janočková^{b,c}, Mária Matejová^a, Eva Konkoľová^b, Helena Paulíková^d, Daniela Lichancová^b, Lenka Júnošová^d, Slávka Hamuláková^a, Ján Imrich^a, Mária Kožurková^{b,c}

^a Department of Organic Chemistry, P. J. Safarik University, Faculty of Science, Moyzesova 11, 04001 Kosice, Slovak Republic

^b Department of Biochemistry, P. J. Safarik University, Faculty of Science, Moyzesova 11, 04001 Kosice, Slovak Republic

^c Biomedical Research Center, University Hospital Hradec Kralove, Sokolovska 581, Hradec Kralove, Czech Republic

^d Department of Biochemistry and Microbiology, Faculty of Chemical and Food Technology, Slovak Technical University, Radlinskeho 9, 81237 Bratislava, Slovak Republic

ARTICLE INFO

Keywords:

Antiproliferative
Diphenylamine
DNA minor groove binder
DNA binding study

ABSTRACT

Nonsteroidal anti-inflammatory drugs (NSAIDs) are the most widely used drugs in the world but some NSAIDs such as diclofenac and tolfenamic acid display levels of cytotoxicity, an effect which has been attributed to the presence of diphenylamine contained in their structures. A novel series of diphenylamine derivatives were synthesised and evaluated for their cytotoxic activities and proliferation inhibition. The most active compounds in the cytotoxicity tests were derivative **6g** with an IC_{50} value of $2.5 \pm 1.1 \times 10^{-6}$ M and derivative **6f** with an IC_{50} value of $6.0 \pm 3.0 \times 10^{-6}$ M (L1210 cell line) after 48 h incubation. The results demonstrate that leukemic L1210 cells were much more sensitive to compounds **6f** and **6g** than the HEK293T cells ($IC_{50} = 35 \times 10^{-6}$ M for **6f** and $IC_{50} > 50 \times 10^{-6}$ M for **6g**) and NIH-3T3 ($IC_{50} > 50 \times 10^{-6}$ M for both derivatives). The IC_{50} values show that these substances may selectively kill leukemic cells over non-cancer cells. Cell cycle analysis revealed that a primary trend of the diphenylamine derivatives was to arrest the cells in the G_1 -phase of the cell cycle within the first 24 h. UV-visible, fluorescence spectroscopy and circular dichroism were used in order to study the binding mode of the novel compounds with DNA. The binding constants determined by UV-visible spectroscopy were found to be in the range of $2.1\text{--}8.7 \times 10^4 \text{ M}^{-1}$. We suggest that the observed trend for binding constant K is likely to be a result of different binding thermodynamics accompanying the formation of the complexes.

1. Introduction

Nonsteroidal anti-inflammatory drugs (NSAIDs) are the most widely used drugs in the world [1], but some NSAIDs such as diclofenac and tolfenamic acid display levels of cytotoxicity, an effect which has been attributed to the presence of diphenylamine contained in their structures (Fig. 1). There is some structural resemblance between the diphenylamine core and DNA minor groove binders, and therefore we synthesized a series of diphenylamine derivatives (**6a–6g**) in order to test their cytotoxic activity and their DNA binding ability (Fig. 1) [1]. The minor groove has a helical curvature which can also vary slightly depending on the sequence, so agents with unfused heterocyclic systems which bind to the minor groove must therefore have a concave shape that complements that of the groove [2]. Small molecules which bind to genomic DNA and which are easily accessible to chromosomal DNA have proven to be effective anticancer therapeutic agents, and therefore researchers continue to be interested in designing pharmacophores which are capable of interacting with DNA [3]. The modes

through which this interaction occurs include intercalation between adjacent base pairs, and intrusion into the minor and major grooves. Intercalation and minor groove binding are the predominant DNA-binding modes of small ligands [4–6].

In this report, we present the results of our assays showing that diphenylamino carboxylic acid derivatives **6a–6g** demonstrate interesting levels of antiproliferative activity with interaction with DNA through groove-binding. The IC_{50} values obtained for the compounds also show that novel derivatives **6f** and **6g** may selectively kill leukemic cells over non-cancer cells.

2. Results and discussions

2.1. Chemistry

Derivatives **6a–6g** were synthesized using the following reaction pathway (Scheme 1) [7]. 4-Acetamido-2-chlorobenzoic acid (**3**) was prepared with a yield of 65% through the oxidation of 4-acetamido-2-

* Corresponding author.

E-mail address: ladislav.janovec@upjs.sk (L. Janovec).

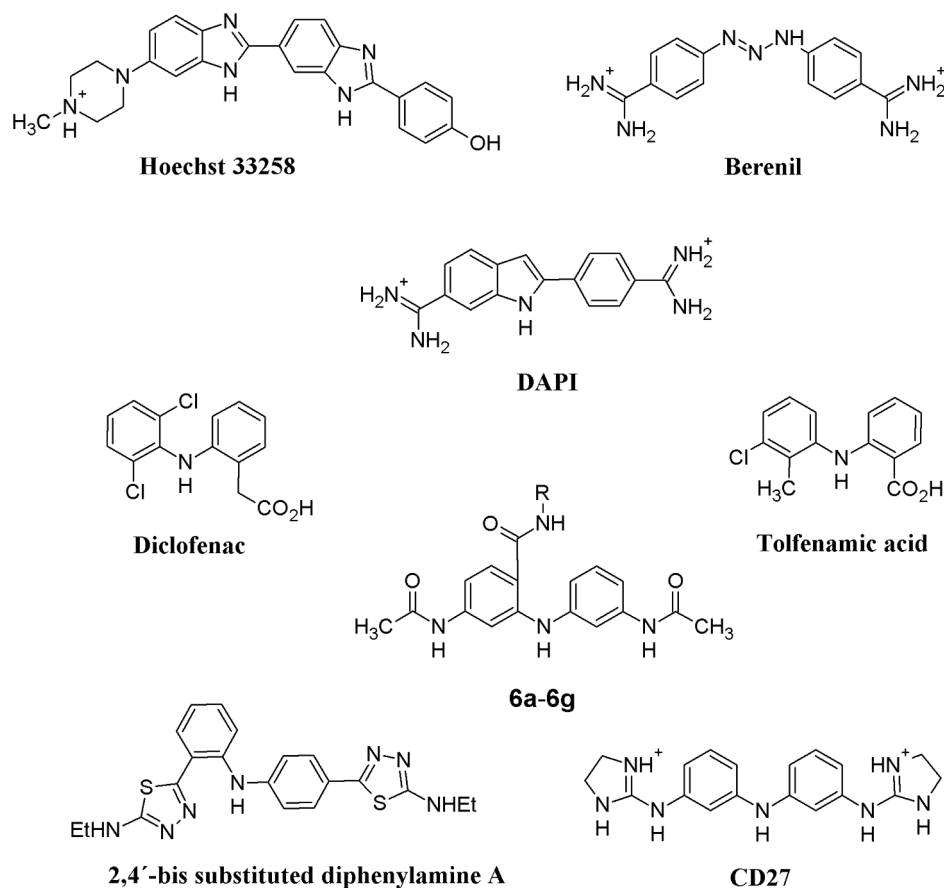


Fig. 1. The structures of DNA minor groove binders **Hoechst 3325**, **Berenil**, **DAPI**, the diphenylamine derivative **A** with antitumor activity, and DNA minor groove binding ability **CD27**.

chlorotoluene (**2**) with KMnO_4 . Compound **2** was obtained by the acetylation of 4-amino-2-chlorotoluene (**1**). Substituted acid **5** was synthesized through the coupling of 4-acetamido-2-chlorobenzoic acid (**3**) with 3-aminoacetanilide (**4**) in ethoxyethanol in the presence of a catalytic amount of copper and copper(I) oxide. Amides **6a–6g** were synthesised through the reaction of amines with carboxylic acid **5** in DMF with the addition of carbonyldiimidazole.

3. Biology

3.1. Cytotoxicity

The anticancer activity of the novel derivatives was also studied by evaluating the cytotoxicity of the compounds against leukemic cells and non-cancer cells *in vitro*. The results presented in **Table 1** demonstrate that the leukemic L1210 cells were more sensitive to compounds **6a–6g** than the non-cancer HEK293T and NIH-3T3 cells. The immortalized cells, human embryonic kidney 293 cells (HEK293T) and mouse embryonic fibroblast cells (NIH-3T3) were less sensitive to the tested substances; indeed, the viability of NIH-3T3 cells decreased only at relatively high concentrations of the derivative, in excess of 50×10^{-6} M. The IC_{50} values of derivatives **6f** and **6g** show that these substances may selectively kill leukemic cells over normal cells (**Table 1**). Derivative **6c** with fluorine and methyl substituent **6b** did not display any increased level of biological activity than that displayed by derivative **6a**. However, the replacement of a phenyl with a piperonyl in derivative **6g** led to a dramatic increase in the anticancer potency of this compound, resulting in a level of toxicity 7-times higher than that of derivative **6a**.

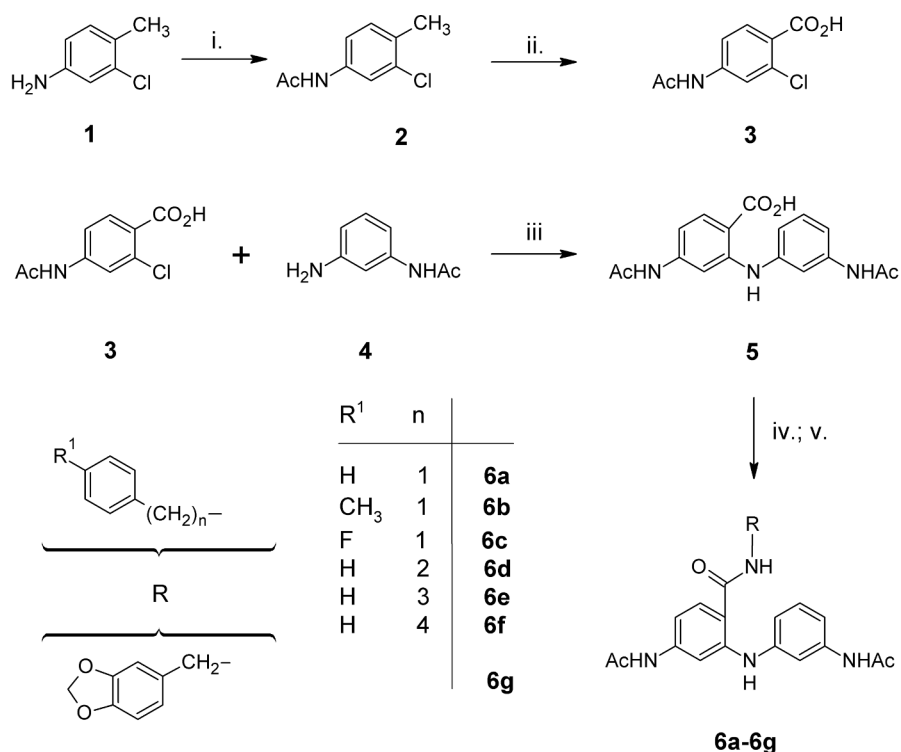
Derivatives **6a** and **6d–6f** form a set of compounds which feature an

elongated alkyl chain. Compound **6f** was found to be the most potent derivative from this set; the high value of log P of **6f** (**Table 1**) enhanced the permeability of this substance and thereby improved its cytostatic activity.

Two of the novel compounds, derivatives **6a** and **6f**, were found to possess different levels of cytotoxicity, lipophilicity and affinity to isolated DNA, therefore the effect of these derivatives on L1210 cells was examined in more detail. The influence of the two derivatives on cell proliferation, plasma membrane integrity and cell cycle, and also the intracellular distribution of the compounds were investigated in order to determine the mechanism of their cytotoxicity.

The proliferation of L1210 cells in the presence of derivatives **6a** and **6f** was determined using the trypan blue method in which the dye is excluded from live cells. As can be seen in **Fig. 2**, a dose dependent decrease was observed in the percentage of viable cells treated with derivatives **6a** and **6f**, but no increase was discerned in the percentage of dead cells (not shown). The results of LDH leakage assays based on the determination of LDH activity in the extracellular medium show that the addition of derivatives **6a** and **6f** at the same concentrations which had inhibited cell proliferation did not induce plasma membrane damage (**Fig. 2**). Derivatives **6a** and **6f** did not induce significant LDH release (activity of LDHex) from the cells. No significant increase was observed in LDH (i.e. the activity of LDHex) from the cells exposed to derivatives **6a** and **6f**.

These two derivatives had also exhibited strong potential for the inhibition of leukemic cell proliferation without inducing cell death, and therefore the morphological changes of L1210 cells incubated with various concentrations of the compounds for 24 h were monitored and compared with the results for untreated control cells. **Fig. 3** shows images of the cells following the addition of propidium iodide and



i: CH₃COCl, Et₃N, MC, 95%; ii: KMnO₄, H₂O, reflux, 2 h, 65%; iii: K₂CO₃, Cu, Cu₂O, ethoxyethanol, reflux, 4 h, 50 %; iv: carbonyldiimidazole, DMF, r.t., 2 h; v: R - NH₂, DMF, r.t., 24 h, 6a (60%), 6b (73%), 6c (68%), 6d (66%), 6e (71%), 6f (72%), 6g (66%).

Scheme 1. Synthesis of derivatives **6a–6g**, amides of substituted diphenylamino carboxylic acid.

Table 1

IC₅₀ values of derivatives **6a–6g** against mouse leukemic cells L1210 and non-cancer cells (HEK293T and NIH-3T3) determined by MTT- assay.

Compounds	IC ₅₀ (× 10 ⁻⁶ M)		
	L1210	HEK293T	NIH-3T3
6a	20 ± 5.3	50 ± 3.2	> 50
6b	31 ± 3.8	38 ± 2.8	> 50
6c	34 ± 4.2	50 ± 5.1	> 50
6d	10 ± 2.4	48 ± 2.4	> 50
6e	10 ± 3.2	26 ± 3.3	> 50
6f	6 ± 3.0	35 ± 4.1	> 50
6g	2.5 ± 1.1	> 50	> 50

The cells were incubated with the substances for 48 h. The tested substances were used in the concentration range of 0–50 × 10⁻⁶ M.

Hoechst 33342 dyes. No significant differences were observed between the morphological features of the treated and untreated cells at lower concentrations, but binuclear cells were observed following treatment with compound **6a** at a concentration of 40 × 10⁻⁶ M. The treated cells did not display any loss of membrane integrity and no induction of necrosis (PI-positive cells) was observed (microphotographs are not shown).

In order to determine the mechanism by which the compounds affect cells, the effect of the two derivatives on cell cycle progression was compared. Cytometric analysis showed that L1210 cells treated with derivatives **6a** and **6f** remained at the G1–S boundary. Both substances induced the accumulation of the cells in the G1 phase of the cell cycle even at concentrations equivalent to IC₅₀ (Fig. 4).

3.2. Intracellular distribution of derivatives **6a** and **6f** and nuclear DNA as a direct target

In order to examine the mechanism of the cytotoxicity of the diphenylamine derivatives against L1210 cells, the intracellular distribution of derivatives **6a** and **6f** was monitored using fluorescence microscopy. Green fluorescence was applied to visualize the compounds and the relatively high concentration of 40 × 10⁻⁶ M was used because of low fluorescence of the compounds. The colocalizations of the substances were also examined using the nucleic acid stain SytoRed (Syto 62 Red). Fig. 5 shows the microphotographs obtained during the assay. The cellular sequestration of derivatives **6a** and **6f** is shown in the strong fluorescence signal primarily observed inside of the nucleus and extending also to the cytosol of the L1210 cells (Fig. 5). The colocalization of Syto Red with compounds **6a** and **6f** confirmed the localization of both of the derivatives in the nuclei of L1210.

In a further assay, cells were treated with the DNA-selective compound Hoechst 33342 in order to provide more information on the interaction of derivatives **6a** and **6f** with nuclear DNA. This dye readily interacts with DNA and is known to act as a minor groove binding ligand [8]. L1210 cells were incubated with different doses of derivatives **6a** or **6f** for 24 h and the treated cells were subsequently washed with PBS and dyed with Hoechst 33342. The stained nuclei in the treated cells revealed that derivatives **6a** and **6f** had reduced the nuclear binding of Hoechst 33342 in a dose dependent manner (Fig. 6).

3.3. DNA binding studies

The newly synthesized derivatives **6a–6g** were investigated for their ability to interact with calf thymus using spectrophotometric titrations in a Tris-HCl buffer. UV-visible absorption titrations were performed in

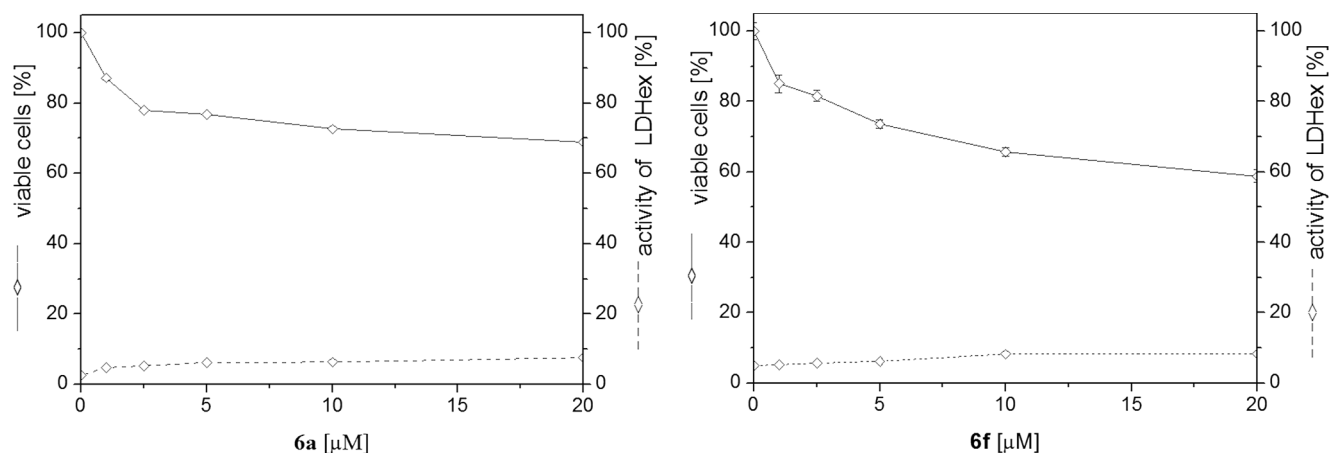


Fig. 2. Effect of derivatives **6a** and **6f** on cell proliferation and plasma membrane integrity. L1210 cells were incubated with compounds **6a** and **6f** for 24 h. The viable cells were counted (trypan blue exclusion test) and the extracellular activity of LDH (LDHex) was determined using LDH leakage assay.

order to ascertain the binding strength of the studied compounds with DNA by monitoring changes in the absorption intensity of the ligand centered bands at a range of around 200–400 nm (Table 2). The absorption spectra of derivatives **6a–6g** in the presence of ctDNA exhibited broad absorption bands in the region of 240–400 nm. The bands of the studied samples exhibit a similarly lower level of hypochromism without any red shift following the incremental addition of ctDNA, a finding which indicates that the compounds bind to DNA *via* a non-intercalative binding mode, possibly through groove-binding. In order to compare the DNA binding affinities of the compounds, binding constants K were determined for each compound using McGhee and von Hippel plots. The binding constants K were estimated to range from 0.21 to $0.87 \times 10^5 \text{ M}^{-1}$. In comparison, binding constants for groove binders generally range from 10^5 to 10^9 M^{-1} [9]. The binding parameters obtained from spectrophotometric analysis are summarized in Table 1.

In order to examine the ability of compounds **6a–6g** to displace EB (ethidium bromide) from its EB-DNA complex, a competitive EB binding study was performed using fluorescence studies. As derivatives **6a–6g** were not excited at wavelengths corresponding to their

maximum absorptions in the absence of ctDNA, the ctDNA samples were pretreated with EB in order to make the interactions more visible. EB forms soluble complexes with DNA and emits intense fluorescence in the presence of ctDNA due to the intercalation of the planar phenanthridinium ring between adjacent base pairs on the double helix [10]. Fluorescence spectra were monitored at a fixed concentration of ctDNA pretreated with EB during titration with increasing concentrations of derivatives **6a–6g**. Figs. 7 and S1 describe the emission spectra of EB bound to DNA in both the presence and absence of the new derivatives. The results of the fluorescence studies demonstrate a quenching of fluorescence intensity of the EB-DNA complex following the addition of increasing concentrations of compounds **6a–6g** (Fig. 7). The results indicate that the compounds can intercalate into the base pairs of DNA and displace EB from the DNA. However, the reduction in the emission intensities of DNA bound EB may be a result of the activity of either DNA intercalators or DNA groove-binders; studies have shown that non-intercalating DNA groove binding agents such as berenil, bisamidines, spermine and spermidine are also capable of displacing EB from DNA [11–13].

In order to identify the binding method of the derivatives to

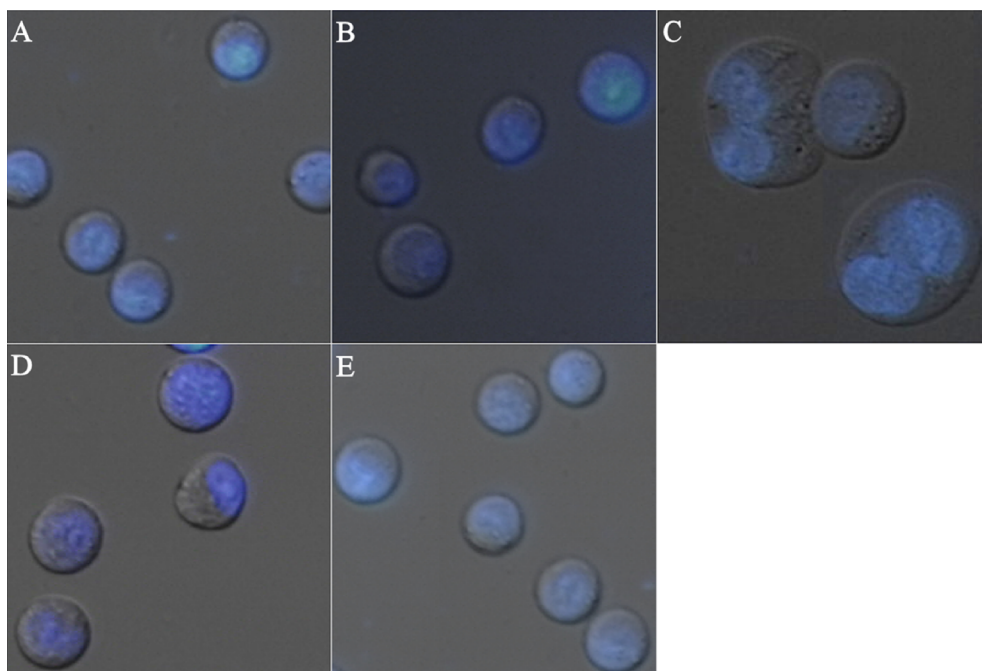


Fig. 3. Representative merged microphotographs of L1210 cells after treatment with derivatives **6a** and **6f** for 24 h. The cells were treated with dual staining of Hoechst 33342/PI to show morphological changes. A-control, B- $20 \times 10^{-6} \text{ M}$ of compound **6a**, C- $40 \times 10^{-6} \text{ M}$ of compound **6a**, D- $20 \times 10^{-6} \text{ M}$ of compound **6f**, E- $40 \times 10^{-6} \text{ M}$ of compound **6f**. Microphotographs of the cells were obtained using an Axio Imager A1 (Zeiss, Germany) fluorescence microscope at a magnification of 40×10 .

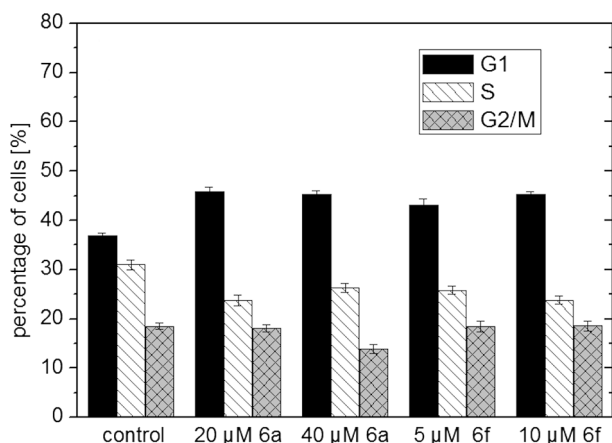


Fig. 4. Cell cycle analysis of mouse leukemic L1210 cells. The cells were incubated with derivatives **6a** and **6f** for 24 h at concentrations equivalent to IC_{50} values or at double this concentration. Histograms were analyzed using BD Accuri C6 Software to determine the percentage of the cells in each phase of the cell cycle.

polymeric ctDNA, CD spectral assays were also performed (Figs. 8 and S2). The DNA region of the CD spectrum shown from 220 to 300 nm is characteristic of the retention of a B-DNA conformation [14]. The CD spectrum of ctDNA is characterized by a positive band at 275 nm (symptomatic of base stacking) and a negative band at 245 nm (an indication of the helicity of the B form of DNA). Ligands which bind to DNA through groove-binding or electrostatic interactions exhibit little or no interference with the helicity and stacking bands at the CD spectrum of ctDNA (Figs. 8 and S2). Intercalators are known to stabilize the B-form of DNA leading to significant changes in both bands [7,15–18], therefore it should be possible to ascertain the specific binding mode which has occurred by observing the changes to the DNA region of CD spectra following interaction between ctDNA and the studied compounds. Whilst the B-DNA conformation was clearly retained, small changes in the bands in the DNA region of the spectrum are difficult to interpret, as induced CD signals from the ligand-based spectroscopic transitions of compounds **6a–6c**, **6f** and **6g** could also fall within this region. In contrast, the spectra of the interaction between

ctDNA and phenylethyl derivative **6d** displayed changes to both the positive and negative bands. Representative CD spectra results of compounds **6a** and **6g** are shown in Figs. 8 and S2.

3.4. Docking study

Previous experiments had suggested that the interactions between the novel derivatives and DNA had occurred in a minor groove-binding mode, therefore docking studies utilizing the X-ray model were performed in order to explore this hypothesis. In addition to docking studies of the novel derivatives, studies were also carried out using the well-known DNA minor groove binder Hoechst 33258 (Id PDB: 127D) in order to verify the accuracy of the docking predictions [19]. The powerful software package AutodockVina was initially used to perform the computations, but attempts to predict correct binding modes using this software were unsuccessful; the AutodockVina predictions of CG track for the main DNA binding sequence of Hoechst 33258 did not match with the AT track which had been shown in the X-ray model (not shown) [20]. On this basis, further studies were performed using Autodock software [21,22]. The combinations of charge assignment were tested in order to ensure higher accuracy in the docking predictions; Gasteiger and PM7 charge assignments were used for Hoechst 33258 in combination with AMBER ff14SB and Gasteiger charge assignments for the oligonucleotide [23,24]. In comparing the RMSD for the X-ray ligand pose and the docking ligand pose, the Gasteiger charge was considered to be the most appropriate assignment for both the receptor and the ligand itself (Figs. S3, S4 and Table S1).

The oligonucleotide in the X-ray model (Id PDB:127D) retains an induction fit in its structure, therefore we designed the docking simulation for Hoechst 33258 with oligonucleotide 5'-d(CGCGAATTCGCG)-3' (OLG) in the canonical B-DNA helix which was included as a building option in the Chimera software package [25–27]. Gasteiger partial charges were also added for the ligand and for the oligonucleotide. This decision was made in order to exclude any possible influence of the induction fit on the accuracy of the docking study. A visual inspection of the result shows that the Autodock software was able to correctly reproduce the preference of Hoechst 33258 for an AATT tract with the correct orientation (Fig. 9A).

The possibility of the sequence specific binding of derivatives **6f** and **6g** to DNA was examined using the same details in docking simulations

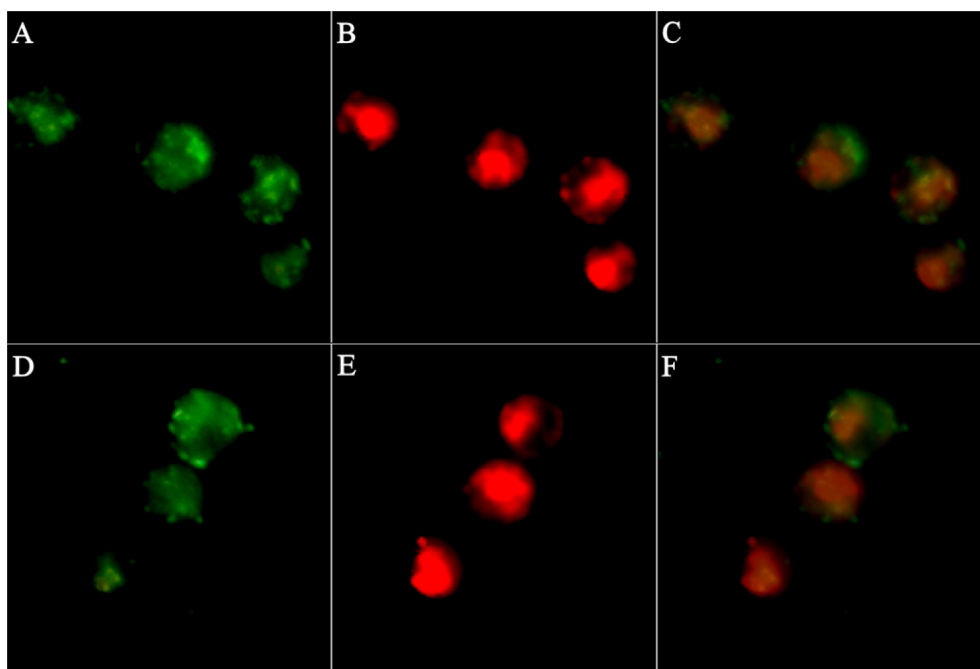


Fig. 5. Intracellular localization of derivatives **6a** and **6f**. L1210 cells were incubated with compound **6a** A–C and compound **6f** D–F (40×10^{-6} M) for 24 h. Intracellular localization of the substance was investigated using green fluorescence and the colocalization of the substance with nucleic acid stain SytoRed was monitored with an Axio Imager A1 (Zeiss, Germany) fluorescence microscope at a magnification of 63×10 .

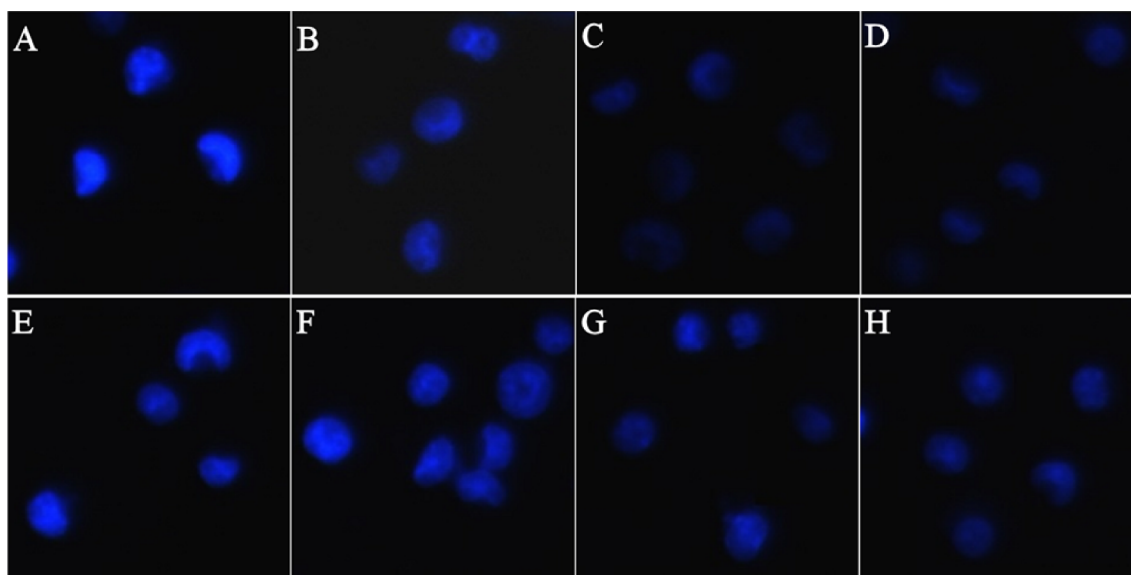


Fig. 6. Dyeing of L1210 cell nuclei with Hoechst 33,342 after incubation with varying concentrations of derivatives **6a** and **6f**. The cells were incubated with derivative **6a** (A-control, B- 2.5×10^{-6} M, C- 5×10^{-6} M, D- 10×10^{-6} M) and derivative **6f** (E-control, F- 2.5×10^{-6} M, G- 5×10^{-6} M, H- 10×10^{-6} M) for 24 h. The cells were then dyed with Hoechst 33,342 (11×10^{-6} M, 37 °C, 15 min) and monitored with an Axio Imager A1 (Zeiss, Germany) fluorescence microscope at a magnification of 40×10 .

Table 2
Binding constants and log *P* values of diphenylamine derivatives **6a–6g**.

Compounds	6a	6b	6c	6d	6e	6f	6g
$K (M^{-1}) \times 10^5$	0.56	0.43	0.21	0.39	0.26	0.87	0.44
$\Delta G (kJ.mol^{-1})$	-39.1	-33.1	-16.8	-30.9	-21.7	-49.1	-33.6
Log <i>P</i> *	2.8	3.3	3.0	3.2	3.8	4.1	2.8

* Log *P* values for derivatives **6a–6g** were calculated using Molinspiration software (www.molinspiration.com).

with OLN (canonical B-DNA helix) as a receptor (Fig. 9B and C). While it might be expected that the derivatives would show an affinity for AATT sequence over GC sequences, compounds **6f** and **6g** did not form any specific highly populated binding cluster within the AATT sequence. In contrast, the docking simulation of Hoechst 33258 shows a huge populated cluster which resembles a binding mode nearly identical to that shown in the x-ray complex. This outcome might be ascribed to the high flexibility of the ligand structure permitting a wide spectrum of possible binding interactions between ligands and oligonucleotides.

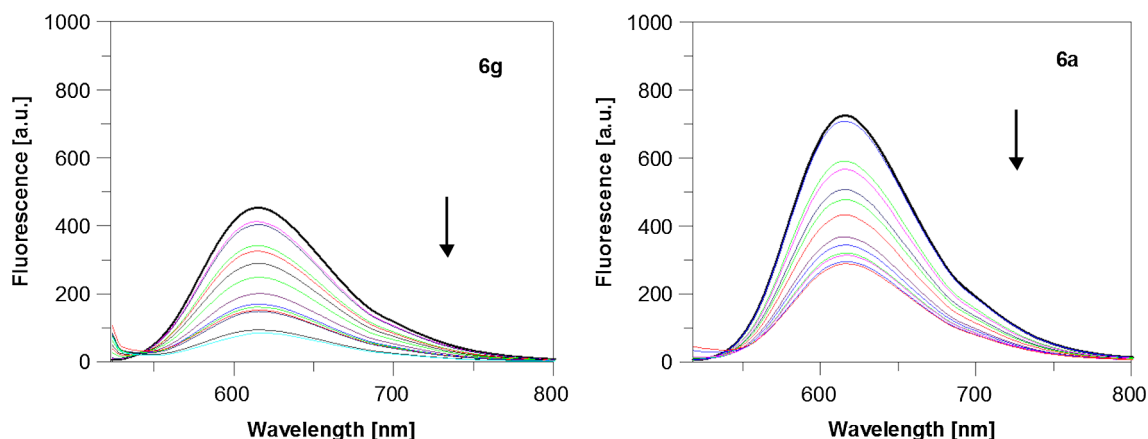


Fig. 7. Emission fluorescence spectra EB bound to DNA (1.65×10^{-5} M) (upper line) in the presence of acridine derivatives **6a** and **6g** (4.97×10^{-5} M) ($c = 0-4.6 \times 10^{-4}$ M) in a 0.01 M Tris-HCl buffer (pH 7.4, 24 °C). The arrow indicates the changes in fluorescence at increasing concentrations of samples.

3.5. Molecular dynamics – A docking like study

Our closer analysis of the relationship between lipophilicity and binding constant *K* (Table 1) reveals a mutual linear correlation within derivatives **6a**, **6d**, **6e**. As Fig. 10 shows, the constant *K* decreases in an almost linear manner with increasing numbers of methylene groups in the derivatives.

However, the results for derivative **6f** did not follow this trend, and the *K* value for this derivative was the highest recorded in the assay. In terms of the correlation observed for the other derivatives, we would predict a binding constant *K* of value around $0.12 \times 10^5 M^{-1}$ for derivative **6f**, but the experimentally determined value of $0.87 \times 10^5 M^{-1}$ is more than seven times higher than expected. In order to find an explanation for such a large discrepancy, we decided to employ methods of computational chemistry at the molecular mechanic (MD) level of theory, using an Amber force field to perform a docking-like study with MD simulations.

A docking pose of the **6f**-OLG complex was used to provide a model for the MD study (Fig. 9B). The phenylbutyl chain was shortened to build up DNA interaction models for derivatives **6a**, **6d** & **6e**. Each MD simulation consisted of three steps within a Generalized Born implicit

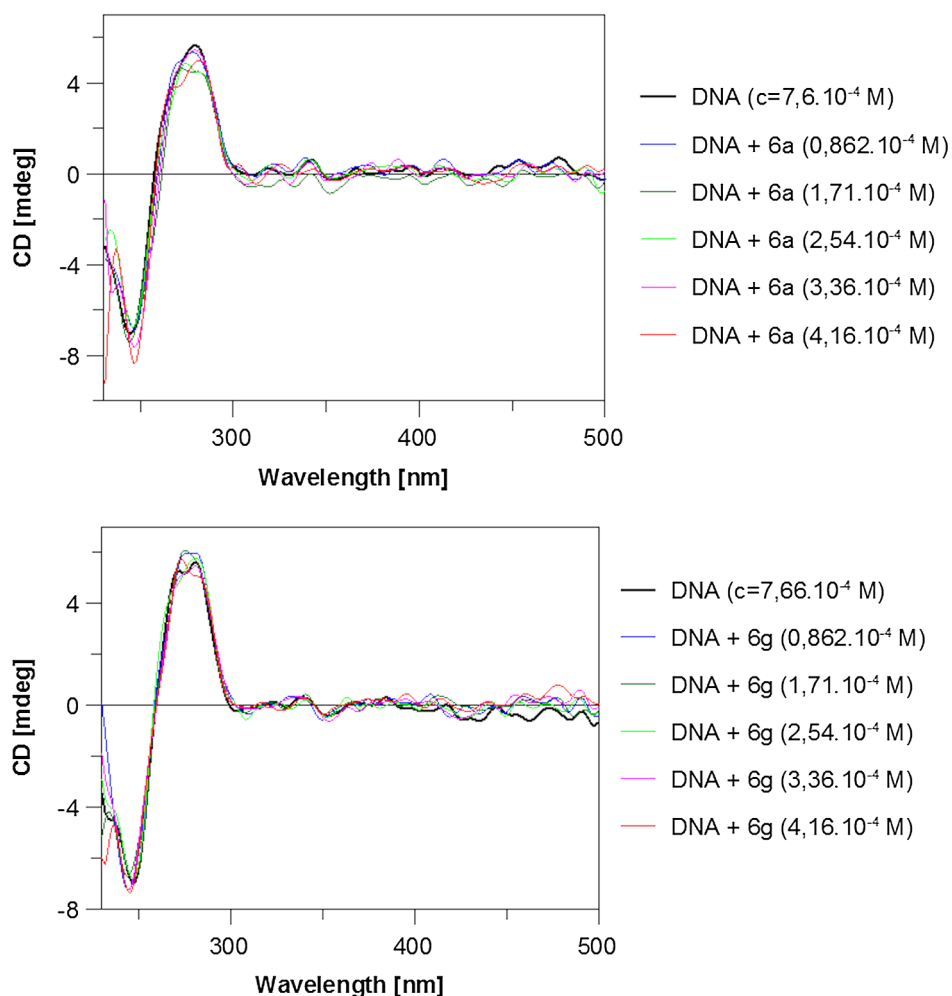


Fig. 8. Circular dichroism spectra of ctDNA (7.66×10^{-4} M) in the absence and presence of derivatives **6a** and **6g** (8.26×10^{-6} M) in a 0.01 M Tris-HCl buffer (pH 7.4, 24 °C). DNA free solutions are shown with black lines and DNA solutions in the presence of the studied derivatives are shown in colored lines.

solvent model using NAMD software. The initial step was the minimization of the ligand–OLG complex, followed by an MD run to eliminate any resulting steric distortion. This relaxed structure was then subjected to minimization and the obtained complex geometry was used for the ligand–oligonucleotide interaction studies (Fig. 11).

In order to analyze the relationship between the structure of the derivatives and their Gibbs' free energies, we used Eq. (1) which consists of energy terms associated with the partial energy changes in the complex formation [28,29]. Definitions of the free energy terms are provided in Supplementary Materials.

$$\Delta G_{obs} = \Delta G_{conf} + \Delta G_{t+r} + \Delta G_{hyd} + \Delta G_{pe} + \Delta G_{mol}, \quad (1)$$

The formation of the ligand–OLG complex was examined in terms of the binding energy change ΔE_{bind} , the interaction energy change ΔE_{inter} and the energy change of the hydrophobic transfer ΔG_{hyd} . The approximate value of ΔG_{hyd} was derived from the change in heat capacity ΔC_p using the calculation of $\Delta G_{hyd} = 80 (\pm 10) \cdot \Delta C_p$. The change in thermal capacity can be estimated from the change in the polar and nonpolar surfaces of OLG, ligand and complex during interactions based on the linear correlation $\Delta C_p = 0.382 (\pm 0.026) \cdot A_{np} - 0.121 (\pm 0.077) \cdot A_p$. Definitions of individual components are provided in Supplementary Materials.

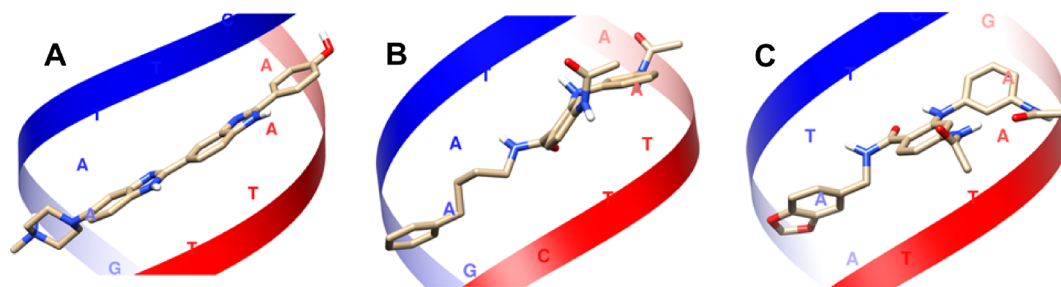


Fig. 9. Docking simulations of putative binding poses of Hoechst 33258 (A), derivative **6f** (B) and derivative **6g** (C) with 5'-d(CGCGAATTCGCG)-3' (canonical B-DNA helix) as the receptor. Simulation performed using Autodock software. Base pairs of the oligonucleotide are depicted as a 1-letter code only and backbones are presented in a red-blue ribbon style. Nonpolar ligand's hydrogens are omitted for clarity. Colors of structures: hydrogen - white, oxygen - red, nitrogen - blue, carbon - grey. Image prepared using Chimera software [25].

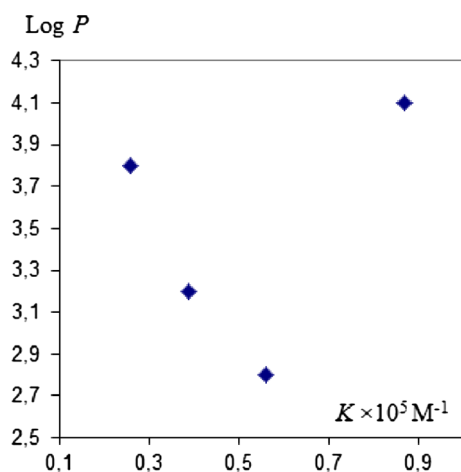


Fig. 10. Relationship of lipophilicity (Log P) and ctDNA binding constants for derivatives **6a** & **6d–6f** ($K/10^5 M^{-1}$) obtained from spectrophotometry.

Coordinates from MD simulations for ligand–OLG complexes and their related components were used to calculate ΔC_p from changes in SASA (Table 3). In order to verify the accuracy of this approach, ΔC_p values for the Hoechst 33258–OLG complex were calculated using x-ray coordinates (PDB ID: 127D) and compared with ΔC_p values obtained from the MD simulation coordinates of the same complex (Table 3). The change in thermal enthalpy calculated from the MD coordinates is $-194.7 \text{ cal. mol}^{-1} \cdot \text{K}^{-1}$ and is in good agreement with the value of $-184.5 \text{ cal. mol}^{-1} \cdot \text{K}^{-1}$ obtained from the x-ray coordinates. It should be noted that ΔC_p values of $-276 (\pm 38)$ or $-259 (\pm 36) \text{ cal. mol}^{-1} \cdot \text{K}^{-1}$ were calculated for the Hoechst 33258–d(CGCA3T3GCG)₂ complex depending on used x-ray structure. The ΔC_p value determined using microcalorimetry was $-300 (\pm 50) \text{ cal. mol}^{-1} \cdot \text{K}^{-1}$.

The binding energy ΔE_{bind} of the complex was determined as a gap of the complex internal energy E_{Complex} and its components, OLG (E_{OLG}) and ligand (E_{Ligand}) (Table 4). The interaction energy ΔE_{Inter} of the complex was calculated using the NAMD module in VMD software as the sum of electrostatic and non-binding interactions (Table 5).

From the values shown in Fig. 12, there is a clear decreasing trend of ΔG_{hyd} that correlates with the increasing proportion of the ligands' non-polar SASA which interacts with the DNA upon ligand binding (Table 3).

A similar trend can be observed for interaction energy ΔE_{Inter} , possibly arising from the increase in van der Waals non-bonding interactions due to the extension of the phenylalkyl chain (Fig. 13B, Table 5).

An analogous correlation is also evident for the complex binding

Table 3
Summary of changes of solvent accessible surface areas (SASAs), heat capacity (ΔC_p), hydrophobic free energy (ΔG_{hyd}).

Ligand–OLG complex	ΔA_p^b (\AA^2)	ΔA_{np}^b (\AA^2)	ΔC_p^c (Cal/mol. K)	ΔG_{hyd}^d (Kcal/mol)
6a ^a	–175.8	–584.4	–202.0	–16.2
6d ^a	–185.9	–642.1	–222.8	–17.8
6e ^a	–164.1	–665.6	–234.4	–18.8
6f ^a	–167.1	–698.2	–246.5	–19.7
Hoechst 33258 [*]	–269.1	–568.1	–184.5	–14.8
Hoechst 33258 ⁺	–152.6	–558.1	–194.7	–15.6

^a Putative mode of interaction with 5'-d(CGCGAATTCGCG)-3' (OLG).

^b Changes of nonpolar (np) and polar (p) SASAs per intercalation calculated using equations $\Delta A_{np} = A_{np}(\text{complex}) - [A_{np}(\text{free DNA}) + A_{np}(\text{free ligand})]$ and $\Delta A_p = A_p(\text{complex}) - [A_p(\text{free DNA}) + A_p(\text{free ligand})]$, resp., from data shown in Tables S2, S3.

^c Calculated using the equation $\Delta C_p = 0.382 (\pm 0.026) \cdot \Delta A_{np} - 0.121 (\pm 0.077) \cdot \Delta A_p$.

^d Calculated from $\Delta G_{\text{hyd}} = 80 (\pm 10) \cdot \Delta C_p$.

^{*} Coordinates obtained from x-ray structure (PDB ID: 127D).

⁺ Coordinates obtained from MD simulation run.

Table 4
Summary of changes in electrostatic internal energy (ΔE_{elect}), van der Waals internal energy (ΔE_{vdw}), internal conformation energy (ΔE_{conf}), internal non-bonded energy (ΔE_{nb}) and binding energy (ΔE_{bind}) for the DNA–ligand complex obtained from MD simulations.

Ligand–OLG complex ^a	$\Delta E_{\text{elect}}^b$ (Kcal/mol)	ΔE_{vdw}^c (Kcal/mol)	ΔE_{conf}^d (Kcal/mol)	ΔE_{nb}^e (Kcal/mol)	ΔE_{bind}^f (Kcal/mol)
6a ^a	–0.3	–58.6	24.5	–58.9	–34.4
6d ^a	–0.4	–61.9	24.3	–62.3	–38.0
6e ^a	–0.3	–62.8	23.3	–63.1	–39.8
6f ^a	–0.4	–69.5	29.3	–69.9	–40.6
Hoechst 33258 ⁺	–2.3	–59.5	24.8	–61.8	–37.0

^a Putative mode of interaction.

^b Obtained using the equation $\Delta E_{\text{elect}} = E_{\text{elect}}(\text{complex}) - [E_{\text{elect}}(\text{free OLG}) + E_{\text{elect}}(\text{free ligand})]$ from data shown in Table S4.

^c Obtained using the equation $\Delta E_{\text{vdw}} = E_{\text{vdw}}(\text{complex}) - [E_{\text{vdw}}(\text{free OLG}) + E_{\text{vdw}}(\text{free ligand})]$ from data shown in Table S4.

^d Obtained using the equation $\Delta E_{\text{conf}} = E_{\text{conf}}(\text{complex}) - [E_{\text{conf}}(\text{free OLG}) + E_{\text{conf}}(\text{free ligand})]$ from data shown in Table S4.

^e Obtained using the equation $\Delta E_{\text{nb}} = E_{\text{nb}}(\text{complex}) - [E_{\text{nb}}(\text{free OLG}) + E_{\text{nb}}(\text{free ligand})]$ from data shown in Table S4.

^f Obtained using the equation $\Delta E_{\text{bind}} = E_{\text{bind}}(\text{complex}) - [E_{\text{bind}}(\text{free OLG}) + E_{\text{bind}}(\text{free ligand})]$ from data shown in Table S4.

⁺ Coordinates obtained from MD simulation run.

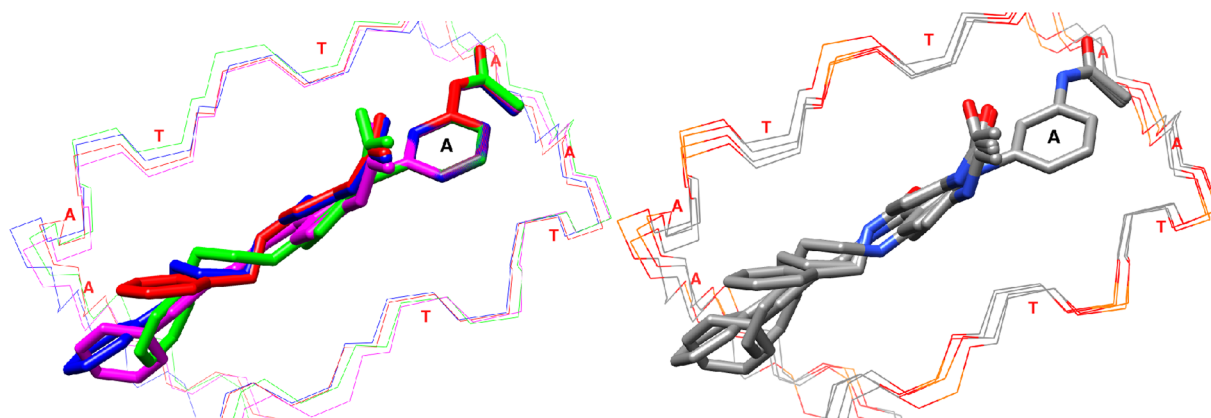


Fig. 11. Putative binding mode of derivatives **6a**, **6d**, **6e** & **6f** within the complex with 5'-d(CGCGAATTCGCG)-3' (OLG). The complexes are superimposed on the structure of the A ring. Color map for structures: red – **6a**–OLG complex; green – **6d**–OLG complex; magenta – **6e**–OLG complex; blue – **6f**–OLG complex. Color map for atoms: red – oxygen; gray – carbon; blue – nitrogen; yellow – phosphorus. Image prepared using Chimera software [25].

Table 5

Summary of changes in electrostatic interaction energy (ΔE_{elect}), van der Waals interaction energy (ΔE_{vdw}) and total interaction energy (ΔE_{inter}) for the complex DNA–ligand obtained from MD simulations.

Ligand–OLG Complex	ΔE_{elect} (Kcal/mol)	ΔE_{vdw} (Kcal/mol)	ΔE_{inter}^b (Kcal/mol)
6a ^a	–0,1	–55,0	–55,1
6d ^a	0,0	–58,0	–58,1
6e ^a	0,0	–61,4	–61,4
6f ^a	0,0	–66,5	–66,5
Hoechst 33258 ⁺	–1,9	–68,6	–70,6

^a Putative mode of interaction.

^b Obtained using an equation $\Delta E_{inter}(\text{complex}) = E_{elect}(\text{complex}) + E_{vdw}(\text{complex})$.

⁺ Coordinates obtained from MD simulation run.

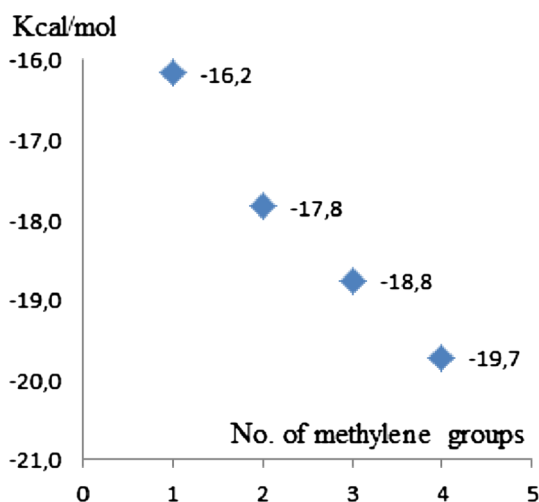


Fig. 12. Relationship of ΔG_{hyd} and number of methylene groups within the structure of derivatives **6a**, **6d**, **6e** & **6f**.

energy ΔE_{bind} , the value of which decreases with increasing numbers of methylene groups in derivatives **6a**, **6d**, **6e** & **6f**. The decrease of ΔE_{bind} is a result of the increase in non-bonding interactions (a decrease in ΔE_{nb} values) which are the driving force of the complex formation (Fig. 13A, Table 4). The main component of the non-bonding interaction ΔE_{nb} is the van der Waals interaction, ΔE_{vdw} . When comparing the energy term ΔE_{vdw} with terms ΔE_{inter} and ΔE_{bind} , there is a clear

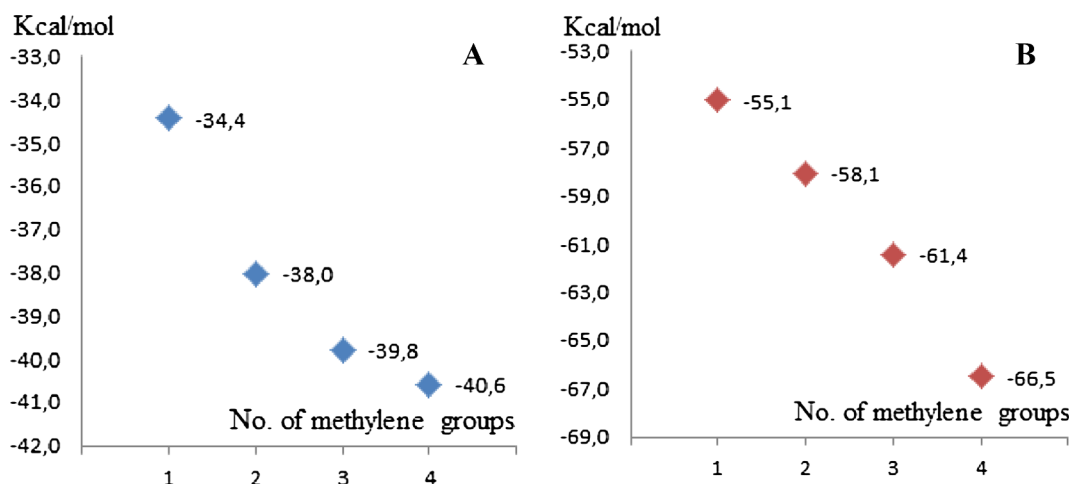


Fig. 13. A: Relationship of ΔE_{bind} and number of methylene groups within the structure of derivatives **6a**, **6d**, **6e**, **6f**. **B:** Relationship of ΔE_{inter} and number of methylene groups within the structure of derivatives **6a**, **6d**, **6e** & **6f**.

proximity of values (Table 4, Table 5) and thus it can be said that $\Delta G_{mol} \cong \Delta E_{nb} \cong \Delta E_{vdw}$.

For derivatives **6a**, **6d** and **6e** the decrease in ΔG_{hyd} and ΔG_{mol} is in contrast to the increase in their ΔG_{obs} values. As is shown in Table 4, the ΔE_{conf} values (formally identified with ΔG_{conf}) are not sufficient to overcome the decrease of energy terms ΔG_{hyd} and ΔG_{mol} that contribute to the overall stability of the complex. A possible explanation of the decrease in complex stability is provided by the energy term ΔG_{t+r} , which is directly linked with the loss of the degree of freedom accompanying complex formation. Since the ΔG_{t+r} value can be calculated as $-\Delta S$, the decrease of the complex stability in the order **6a**, **6d**, **6e** can be attributed to the increase of a loss of entropy ΔS owing to the elongation of the derivatives' alkyl chains.

It is possible to conclude that the increase of hydrophobic surface area and non-bonding interactions due to the elongation of alkyl chains leads to decrease in ΔG_{hyd} and ΔG_{mol} . These energetic terms are overcome by the increase of the loss of entropy ΔS as the consequence of the loss of the degree of freedom upon complex formation.

Although derivative **6f** is an extension of the series of derivatives **6a**, **6d** & **6e**, the conclusion discussed above does not explain the increase in its K value. According to the proposed interaction model, a binding constant K for the **6f**–OLG complex would have a value of $0.12 \times 10^5 \text{ M}^{-1}$, but the constant K obtained in experiments is $0.87 \times 10^5 \text{ M}^{-1}$. Thus, the increase in the complex stability of derivative **6f** cannot be linked to the structural similarity within the bound ligands. One possible explanation could be found in the general thermodynamic effect during the formation of the complex. Therefore the binding of derivative **6f** into the DNA minor groove might lead to the expulsion of site-specifically bound water or cations accompanied by a large favorable entropy term. This may be the main driving force in the reaction and could explain why the binding constant K for derivative **6f**–OLG complex differs from the trend observed for derivatives **6a**, **6d** & **6e**.

This explanation is in accordance with the Hoechst 33258–DNA complex formation where the main driving force is the gain of entropy as the consequence of water expulsion from a minor groove into the bulk solvent. The explanation may also point to the fact that isostructural does not mean isoenergetic, and therefore a small change in the alkyl chain might lead to a significant change in the binding thermodynamics.

4. Conclusion

A series of new derivatives with a diphenylamino carboxylic acid framework were synthesised and evaluated for their cytotoxic activities

and proliferation inhibition. The most active compounds in the cytotoxicity tests were derivative **6g** with an IC_{50} value of $2.5 \pm 1.1 \times 10^{-6}$ M and derivative **6f** with an IC_{50} value of $6.0 \pm 3.0 \times 10^{-6}$ M (L1210 cell line) after 48 h incubation. The selective cytotoxicity to leukemia L1210 cells was also confirmed, and was found to be higher than that observed against HEK293T and NIH-3T3 cells. Cell cycle analysis revealed that a primary trend of the diphenylamine derivatives was to arrest the cells in the G1-phase of the cell cycle within the first 24 h. UV-visible, fluorescence spectroscopy and circular dichroism were used in order to study the binding mode of the novel compounds with DNA. The binding constants determined by UV-visible spectroscopy were found to be in the range of $0.21\text{--}0.87 \times 10^5 \text{ M}^{-1}$. The results suggest that the compounds interact with DNA through groove binding. Additional in silico DNA binding studies with experimental findings revealed differences between isostructural and isoenergetic relationships in the series of studied derivatives.

5. Experimental

5.1. Chemistry

All chemicals and reagents were reagent grade and were used without further purification. ^1H (400 MHz, 600 MHz) and ^{13}C (100 MHz, 150 MHz) NMR spectra were measured on a Varian Mercury Plus or a Varian VNMR NMR spectrometers at room temperature in DMSO- d_6 using TMS as an internal standard (0 ppm for both nuclei). Melting points were determined with a Koffler hot-stage apparatus and are uncorrected. Elemental analyses were performed on a Perkin-Elmer analyzer CHN 2400. Reactions were monitored with thin-layer chromatography (TLC) using Silufol plates with detection at 254 nm. Preparative column chromatography was performed using a Kieselgel Merck 60 column, type 9385 (grain size 250 nm). Chlorotoluene **2**, acid **3**, **5** and products **6a–6f** were prepared according to the published procedures [7]. Compounds **2**, **3** and **5** are described in Supplementary Material.

5.1.1. General synthesis of 4-(acetylamino)-2-[[3-(acetylamino)phenyl]amino]-N-substituted benzamide **6a–6g**

A mixture of derivative **5** (1 g, 3.05 mmol) and carbonyldiimidazole (1.5 g, 9.15 mmol) in dimethylformamide (10 mL) was mixed at room temperature. After the reaction was finished (approximately 2 h, TLC methanol - ethyl acetate (6:1 v/v)), appropriate amine (9.51 mmol) was added. The reaction mixture was stirred at room temperature for an additional 24 h and subsequently poured into distilled water. Precipitated crude products **6a–6g** were filtered off and dried overnight. Derivatives **6a–6g** were purified by column chromatography using a mobile phase methanol - ethyl acetate (1:6 v/v) and crystallized from ethanol. Numbering of atoms for **6a–6g** in NMR assignments corresponds to the numbering of the final product **6f** and is shown in Fig S5.

5.1.1.1. 4-(Acetylamino)-2-[[3-(acetylamino)phenyl]

amino]-N-benzylbenzamide (**6a**). Yield: 60%, gray solid, mp: 214–216 °C. ^1H NMR (400 MHz, DMSO- d_6) σ , ppm 10.00 (s, 1H, NH), 10.00 (s, 1H, Ph-NH-Ph), 9.89 (s, 1H, NH $^{\prime}$), 8.98 (t, 1H, NH, $J = 6.0$ Hz), 7.69 (d, 1H, H-6, $J = 8.4$ Hz), 7.54 (d, 1H, H-3, $J = 1.6$ Hz), 7.41 (s, 1H, H-2 $^{\prime}$), 7.33 – 7.32 (m, 4H, H-2 $^{\prime\prime}$, 6 $^{\prime\prime}$, H-3 $^{\prime\prime}$, 5 $^{\prime\prime}$), 7.25 – 7.21 (m, 3H, H-4 $^{\prime\prime}$, H-4 $^{\prime\prime}$, 5 $^{\prime\prime}$), 7.13 (dd, 1H, H-5, $J = 8.4$ Hz, $J = 1.6$ Hz), 6.89 – 6.86 (m, 1H, H-6 $^{\prime}$), 4.45 (d, 2H, CH $_2$, $J = 6.0$ Hz), 2.03 (s, 3H, CH $_3$), 2.01 (s, 3H, CH $_3$).

^{13}C NMR (100 MHz, DMSO- d_6) σ , ppm 168.6 (C=O), 168.5 (C=O), 168.3 (C=O), 145.6 (C2), 142.6 (C4), 141.6 (C1 $^{\prime}$), 140.4 (C3 $^{\prime}$), 139.6 (C1 $^{\prime\prime}$), 129.5 (C6, C5 $^{\prime}$), 128.3 (C3 $^{\prime\prime}$, C5 $^{\prime\prime}$), 127.2 (C2 $^{\prime\prime}$, C6 $^{\prime\prime}$), 126.7 (C4 $^{\prime\prime}$), 114.3 (C6 $^{\prime}$), 112.8 (C4 $^{\prime}$), 112.4 (C1), 110.7 (C2 $^{\prime}$), 108.6 (C5), 104.2 (C3), 42.3 (CH $_2$), 24.1 (CH $_3$), 24.1 (CH $_3$). Anal. Calcd for C $_{24}$ H $_{24}$ N $_4$ O $_3$

(416.47): 69.21% C, 5.81% H, 13.45% N; found: 69.40% C, 5.67% H, 13.60% N.

5.1.1.2. 4-(Acetylamino)-2-[[3-(acetylamino)phenyl]

amino]-N-[(4-methylphenyl)methyl] benzamide (**6b**). Yield = 73%, gray solid, mp = 145–147 °C. ^1H NMR (400 MHz, DMSO- d_6) σ , ppm 10.00 (s, 1H, NH), 9.99 (s, 1H, Ph-NH-Ph), 9.89 (s, 1H, NH $^{\prime}$), 8.94 (t, 1H, NH, $J = 6.0$ Hz), 7.68 (d, 1H, H-6, $J = 8.4$ Hz), 7.54 (d, 1H, H-3, $J = 1.6$ Hz), 7.41 (s, 1H, H-2 $^{\prime}$), 7.22 – 7.20 (m, 4H, H-4 $^{\prime\prime}$, 5 $^{\prime\prime}$, H-2 $^{\prime\prime}$, 6 $^{\prime\prime}$), 7.15 – 7.13 (m, 3H, H-5, H-3 $^{\prime\prime}$, 5 $^{\prime\prime}$), 6.89 – 6.86 (m, 1H, H-6 $^{\prime}$), 4.40 (d, 2H, CH $_2$, $J = 6.0$ Hz), 2.27 (s, 3H, CH $_3$), 2.03 (s, 3H, CH $_3$), 2.02 (s, 3H, CH $_3$).

^{13}C NMR (100 MHz, DMSO- d_6) σ , ppm 168.6 (CO), 168.5 (CO), 168.3 (CO), 145.6 (C2), 142.6 (C4), 141.6 (C1 $^{\prime}$), 140.4 (C3 $^{\prime}$), 136.6 (C1 $^{\prime\prime}$), 135.8 (C4 $^{\prime}$), 129.5 (C5 $^{\prime}$), 129.5 (C6), 128.8 (C3 $^{\prime\prime}$, C5 $^{\prime\prime}$), 127.2 (C2 $^{\prime\prime}$, C6 $^{\prime\prime}$), 114.3 (C6 $^{\prime}$), 112.8 (C4 $^{\prime}$), 112.5 (C1), 110.7 (C2 $^{\prime}$), 108.7 (C5), 104.2 (C3), 42.1 (CH $_2$), 24.2 (CH $_3$), 24.1 (CH $_3$), 20.7 (CH $_3$). Anal. Calcd for C $_{25}$ H $_{26}$ N $_4$ O $_3$ (430.49): 69.75% C, 6.09% H, 13.01% N; found: 70.01% C, 6.17% H, 12.83% N.

5.1.1.3. 4-(Acetylamino)-2-[[3-(acetylamino)phenyl]

amino]-N-[(4-fluorophenyl)methyl] benzamide (**6c**). Yield = 68%, gray solid, mp = 148–150 °C. ^1H NMR (400 MHz, DMSO- d_6) σ , ppm 10.00 (s, 1H, NH), 9.98 (s, 1H, Ph-NH-Ph), 9.89 (s, 1H, NH $^{\prime}$), 8.99 (t, 1H, NH, $J = 6.0$ Hz), 7.68 (d, 1H, H-6, $J = 8.4$ Hz), 7.55 (d, 1H, H-3, $J = 1.8$ Hz), 7.42 (s, 1H, H-2 $^{\prime}$), 7.38 – 7.34 (m, 2H, H-2 $^{\prime\prime}$, 6 $^{\prime\prime}$), 7.22 – 7.21 (m, 2H, H-4 $^{\prime\prime}$, 5 $^{\prime\prime}$), 7.16 – 7.12 (m, 3H, H-5, H-3 $^{\prime\prime}$, 5 $^{\prime\prime}$), 6.89 – 6.86 (m, 1H, H-6 $^{\prime}$), 4.42 (d, 2H, CH $_2$, $J = 6.0$ Hz), 2.03 (s, 3H, CH $_3$), 2.01 (s, 3H, CH $_3$).

^{13}C NMR (100 MHz, DMSO- d_6) σ , ppm 168.6 (CO), 168.5 (CO), 168.3 (CO), 161.1 (d, C4 $^{\prime}$, $J = 240.0$ Hz), 145.7 (C2), 142.7 (C4), 141.6 (C1 $^{\prime}$), 140.4 (C3 $^{\prime}$), 135.8 (d, C1 $^{\prime\prime}$, $J = 3.0$ Hz), 129.5 (C6, C5 $^{\prime}$), 129.2 (d, C2 $^{\prime\prime}$, C6 $^{\prime\prime}$, $J = 7.5$ Hz), 115.0 (d, C3 $^{\prime\prime}$, C5 $^{\prime\prime}$, $J = 21.0$ Hz), 114.4 (C6 $^{\prime}$), 112.8 (C4 $^{\prime}$), 112.3 (C1), 110.7 (C2 $^{\prime}$), 108.7 (C5), 104.2 (C3), 41.7 (CH $_2$), 24.2 (CH $_3$), 24.1 (CH $_3$). Anal. Calcd for C $_{24}$ H $_{23}$ FN $_4$ O $_3$ (434.46): 66.35% C, 5.34% H, 12.90% N; found: 66.40% C, 5.19% H, 12.69% N.

5.1.1.4. 4-(Acetylamino)-2-[[3-(acetylamino)phenyl]

amino]-N-[2-(phenylethyl)]benzamide (**6d**). Yield = 66%, gray solid, mp = 113–115 °C. ^1H NMR (400 MHz, DMSO- d_6) σ , ppm 9.98 (s, 1H, NH), 9.92 (s, 1H, Ph-NH-Ph), 9.89 (s, 1H, NH $^{\prime}$), 8.51 (t, 1H, NH, $J = 5.4$ Hz), 7.55 (d, 1H, H-6, $J = 8.4$ Hz), 7.52 (s, 1H, H-3), 7.41 (s, 1H, H-2 $^{\prime}$), 7.31 – 7.27 (m, 2H, H-3 $^{\prime\prime}$, 5 $^{\prime\prime}$), 7.25 – 7.23 (m, 2H, H-2 $^{\prime\prime}$, 6 $^{\prime\prime}$), 7.22 – 7.17 (m, 3H, H-4 $^{\prime\prime}$, 5 $^{\prime\prime}$, H-4 $^{\prime\prime}$), 7.12 (d, 1H, H-5, $J = 8.4$ Hz), 6.87 – 6.85 (m, 1H, H-6 $^{\prime}$), 3.47 – 3.43 (dd, 2H, CH $_2$ –1), 2.83 (t, 2H, CH $_2$ –2, $J = 7.2$ Hz), 2.03 (s, 3H, CH $_3$), 2.01 (s, 3H, CH $_3$).

^{13}C NMR (100 MHz, DMSO- d_6) σ , ppm 168.6 (CO), 168.5 (CO), 168.3 (CO), 145.4 (C2), 142.5 (C4), 141.7 (C1 $^{\prime}$), 140.4 (C3 $^{\prime}$), 139.5 (C1 $^{\prime\prime}$), 129.5 (C5 $^{\prime}$), 129.3 (C6), 128.7 (C2 $^{\prime\prime}$, C6 $^{\prime\prime}$), 128.3 (C3 $^{\prime\prime}$, C5 $^{\prime\prime}$), 126.1 (C4 $^{\prime}$), 114.2 (C6 $^{\prime}$), 113.0 (C1), 112.7 (C4 $^{\prime}$), 110.6 (C2 $^{\prime}$), 108.7 (C5), 104.4 (C3), 40.7 (CH $_2$ –1), 35.1 (CH $_2$ –2), 24.2 (CH $_3$), 24.1 (CH $_3$). Anal. Calcd for C $_{25}$ H $_{26}$ N $_4$ O $_3$ (430.49): 69.75% C, 6.09% H, 13.01% N; found: 69.81% C, 6.19% H, 13.39% N.

5.1.1.5. 4-(Acetylamino)-2-[[3-(acetylamino)phenyl]

amino]-N-[3-(phenylpropyl)]benzamide (**6e**). Yield = 71%, gray solid, mp = 123–125 °C. ^1H NMR (400 MHz, DMSO- d_6) σ , ppm 9.98 (s, 1H, NH), 9.92 (s, 1H, Ph-NH-Ph), 9.88 (s, 1H, NH $^{\prime}$), 8.43 (t, 1H, NH, $J = 6.0$ Hz), 7.60 (d, 1H, H-6, $J = 8.4$ Hz), 7.53 (s, 1H, H-3, $J = 1.6$ Hz), 7.40 (s, 1H, H-2 $^{\prime}$), 7.28 – 7.23 (m, 2H, H-3 $^{\prime\prime}$, 5 $^{\prime\prime}$), 7.23 – 7.20 (m, 4H, H-2 $^{\prime\prime}$, 6 $^{\prime\prime}$, H-4 $^{\prime\prime}$, 5 $^{\prime\prime}$), 7.18 – 7.16 (m, 1H, H-4 $^{\prime}$), 7.13 (d, 1H, H-5, $J = 8.4$ Hz), 7.29 – 7.11 (m, 8H), 6.88 – 6.85 (m, 1H, H-6 $^{\prime}$), 3.25 (m, 2H, CH $_2$ –1), 2.63 (t, 2H, CH $_2$ –3, $J = 7.2$ Hz), 2.03 (s, 3H, CH $_3$), 2.01 (s, 3H, CH $_3$), 1.86 – 1.78 (m, 2H, CH $_2$ –2).

^{13}C NMR (100 MHz, DMSO- d_6) σ , ppm 168.6 (CO), 168.5 (CO), 168.3 (CO), 145.3 (C2), 142.4 (C4), 141.8 (C1 $^{\prime}$), 141.7 (C1 $^{\prime\prime}$), 140.4

(C3[′]), 129.5 (C5[′]), 129.4 (C6), 128.3 (C2[′], C6[′]), 128.3 (C3[′], C5[′]), 125.7 (C4[′]), 114.1 (C6[′]), 113.1 (C1), 112.6 (C4[′]), 110.5 (C2[′]), 108.7 (C5), 104.4 (C3), 38.7 (CH₂-1), 32.7 (CH₂-3), 30.7 (CH₂-2), 24.1 (CH₃[′]), 24.1 (CH₃). Anal. Calcd for C₂₆H₂₈N₄O₃ (444.52): 70.25% C, 6.35% H, 12.60% N; found: 70.03% C, 6.44% H, 12.25% N.

5.1.1.6. 4-(Acetylamino)-2-[[3-(acetylamino)phenyl]

amino]-N-[4-(phenylbutyl)]benzamide (**6f**). Yield = 72%, gray solid, mp = 214–216 °C. ¹H NMR (400 MHz, DMSO-*d*₆) σ , ppm 9.98 (s, 1H, NH[′]), 9.97 (s, 1H, Ph-NH-Ph), 9.89 (s, 1H, NH[′]), 8.41 (t, 1H, NH, *J* = 6.0 Hz), 7.58 (d, 1H, H-6, *J* = 8.4 Hz), 7.53 (d, 1H, H-3, *J* = 1.8 Hz), 7.41 (s, 1H, H-2[′]), 7.28 – 7.23 (m, 2H, H-3[′], 5[′]), 7.21 – 7.17 (m, 4H, H-2[′], 6[′], H-4[′], 5[′]), 7.16 – 7.14 (m, 1H, H-4[′]), 7.12 (dd, 1H, H-5, *J*₁ = 8.4, *J*₂ = 1.8), 6.87 – 6.85 (m, 1H, H-6[′]), 3.25 (dd, 2H, CH₂-1, *J*₁ = 7.2, *J*₂ = 1.2), 2.60 (t, 2H, CH₂-4, *J* = 7.2), 2.03 (s, 3H, CH₃[′]), 2.01 (s, 3H, CH₃), 1.60 – 1.57 (m, 2H, CH₂-2), 1.54 – 1.52 (m, 2H, CH₂-3).

¹³C NMR (100 MHz, DMSO-*d*₆) σ , ppm 168.6 (CO[′]), 168.5 (CO), 168.3 (CO[′]), 145.3 (C2), 142.4 (C4), 142.2 (C1[′]), 141.7 (C1[′]), 140.4 (C3[′]), 129.5 (C5[′]), 129.3 (C6), 128.3 (C2[′], C6[′]), 128.2 (C3[′], C5[′]), 125.6 (C4[′]), 114.1 (C6[′]), 113.1 (C1), 112.6 (C4[′]), 110.4 (C2[′]), 108.6 (C5), 104.4 (C3), 38.7 (CH₂-1), 34.8 (CH₂-4), 28.7 (CH₂-2), 28.5 (CH₂-3), 24.1 (CH₃[′]), 24.1 (CH₃). Anal. Calcd for C₂₇H₃₀N₄O₃ (458.57): 70.72% C, 6.59% H, 12.22% N; found: 70.43% C, 6.51% H, 12.17% N.

5.1.1.7. 4-(Acetylamino)-2-[[3-(acetylamino)phenyl]

amino]-N-piperonylbenzamide (**6g**). Yield = 66%, gray solid, mp = 220–222 °C. ¹H NMR (400 MHz, DMSO-*d*₆) σ , ppm 9.99 (s, 1H, NH[′]), 9.98 (s, 1H, Ph-NH-Ph), 9.89 (s, 1H, NH[′]), 8.91 (t, 1H, NH, *J* = 6.0 Hz), 7.66 (d, 1H, H-6, *J* = 8.4 Hz), 7.54 (d, 1H, H-3, *J* = 1.8 Hz), 7.41 (s, 1H, H-2[′]), 7.22 – 7.21 (m, 2H, H-4[′], 5[′]), 7.13 (dd, 1H, H-5, *J* = 8.4, 1.8 Hz), 6.89 (d, 1H, H-4[′], *J* = 1.8 Hz), 6.88 – 6.86 (m, 1H, H-6[′]), 6.85 (d, 1H, H-7[′], *J* = 7.8 Hz), 6.80 (dd, 1H, H-6[′], *J*₁ = 7.8, *J*₂ = 1.8 Hz), 5.97 (s, 2H, CH₂[′]), 4.34 (d, 2H, CH₂, *J* = 6.0 Hz), 2.03 (s, 3H, CH₃[′]), 2.01 (s, 3H, CH₃).

¹³C NMR (100 MHz, DMSO-*d*₆) σ , ppm 168.6 (CO[′]), 168.4 (CO), 168.3 (CO[′]), 147.2 (C3a[′]), 146.0 (C7a[′]), 145.6 (C2), 142.7 (C4), 141.6 (C1[′]), 140.4 (C3[′]), 133.5 (C5[′]), 129.5 (C6, C5[′]), 120.5 (C6[′]), 114.3 (C6[′]), 112.8 (C4[′]), 112.4 (C1), 110.7 (C2[′]), 108.7 (C5), 108.0 (C7[′]), 107.9 (C4[′]), 104.2 (C3), 100.8 (CH₂[′]), 42.2 (CH₂), 24.2 (CH₃[′]), 24.1 (CH₃). Anal. Calcd for C₂₅H₂₄N₄O₅ (460.48): 65.21% C, 5.25% H, 12.17% N; found: 65.10% C, 5.41% H, 12.10% N.

5.2. Biology

The studied derivatives were dissolved in DMSO to a concentration of 4.49×10^{-3} M. Calf thymus sodium salt was purchased from Sigma Aldrich chemicals (Sigma Aldrich, USA). Calf thymus DNA (ctDNA) stock solution was prepared by dissolving 1 mg/mL in a Tris-EDTA buffer (TE buffer contains 1×10^{-2} M Tris-HCl pH 7.4 and 1×10^{-3} M EDTA) at 4 °C overnight. The final concentration of ctDNA was identified spectrophotometrically at 260 nm. The purity of ctDNA was measured as a ratio of the absorption at 260/280 nm and was found to be 1.82, a value which indicates that the ctDNA sample was pure and devoid of protein contamination. All other chemicals and reagents were purchased at reagent grade and were used without further purification. Ethidium bromide, Triton X-100 and dimethyl sulfoxide (DMSO) were obtained from Sigma-Aldrich Chemie (Germany). EDTA, RNase A and proteinase K were purchased from Serva (Germany). All other chemicals were purchased from Lachema (Czech Republic).

5.2.1. Cell culture conditions

Mouse leukemia cell lines L1210 were grown in a RPMI-1640 medium and mouse embryonic fibroblast cell line NIH-3T3 and human embryonic kidney 293 cells HEK293T in DMEM medium. Both media were supplemented with 10% FBS, penicillin (100 units/mL), and

streptomycin (100 μ g/mL). The cells were maintained at 37 °C in a humidified 5% CO₂ atmosphere. NIH-3T3 and HEK293 cells were harvested using a trypsin solution (0.25% trypsin/EDTA). The L1210 and NIH-3T3 cells were obtained from Dr. Ujhazy, Roswell Park Cancer Institute, Buffalo and the human embryonic kidney cells HEK293T from ATCC, Manassas, VA, USA.

5.2.2. MTT assay

Cell viability was determined using the MTT microculture tetrazolium assay method which has been described previously [30]. Cells (25×10^4 /mL) were incubated with derivatives **6a–6g** ($0–50 \times 10^{-6}$ M) for 48 h and the viability of cells was determined. Absorbance was then measured at 570 and 630 nm as a background using a microplate reader (Synergy H1 Hybrid). The IC₅₀ value was determined from the dose-response curves of every cell line.

5.2.3. Trypan blue exclusion test

Cell proliferation and the cytotoxic potential of compounds were determined using a trypan blue dye exclusion test. Cells were seeded (0.15×10^6 cells/mL) in Petri dishes and derivatives **6a** and **6f** ($0–20 \times 10^{-6}$ M) were added after 24 h. Cell proliferation was then checked after 24 h.

5.2.4. LDH leakage assay

A lactate dehydrogenase assay (LDH) was performed using the method described by Grivell and Berry [31]. The cells (0.15×10^6 cells/mL) were treated with derivatives **6a–6f** ($0–20 \times 10^{-6}$ M) and after 24 h, 100×10^{-6} L of the sample from the growth medium of L1210 cells was added to a 1×10^{-3} L cuvette containing 0.9×10^{-3} L of a reaction mixture to yield a final concentration of 1×10^{-3} M pyruvate, 0.15×10^{-3} M NADH, and 100×10^{-3} M phosphate buffer (pH 7.4). The incubation mixture was mixed thoroughly and the absorbance was measured at 366 nm for 3 min. The activity of LDH was also measured in cell lysate.

5.2.5. Cytomorphological changes

Cells (1.5×10^5 /mL) were treated with derivatives **6a** and **6f** ($0–40 \times 10^{-6}$ M) and incubated at 37 °C for 24 h. After incubation, the cells were washed with PBS and stained with Hoechst 33,342 for the visualization of the cell nuclei (10×10^{-6} M, 10 min) and with propidium iodide (PI, 1 mg/mL, 10 min) to visualize the damaged membrane integrity of the cells. Changes in cell morphology and damage to plasma membrane integrity (PI positive cells) were observed using an Axio ANO Imager A1 optical and fluorescence microscope (Zeiss, Germany).

5.2.6. Cell cycle analysis

Cells (0.5×10^6 /mL) were washed with PBS after incubation (6–24 h) with derivative **6a** (1, 5 and 10×10^{-6} M) or derivative **6f** (1, 2.5 and 5×10^{-6} M). The cells were subsequently fixed with ethanol and stored at -20 °C. Prior to measurements, RNase (0.2 mg/mL) was added for 20 min at 37 °C. Afterwards, the cells were stained with PI (0.05 mg/mL) and analyzed using an Accuri C6 flow cytometer.

5.2.7. Intracellular distribution of derivatives **6a** and **6f** – Colocalization with SytoRed

L1210 cells (0.5×10^6) were treated with 40×10^{-6} M of derivatives **6a** and **6f** (37 °C) for 2 h and then the samples were labeled with SytoRed (0.1×10^{-6} M, 35 min) in order to visualize the cell nuclei. After incubation with SytoRed, the cells were washed twice with PBS and immediately visualized using an Axio ANO Imager A1 fluorescence microscope (Zeiss, Germany).

5.2.8. UV-visible absorption measurements

The UV-Vis absorption spectra (200 – 450 nm) of a fixed concentration of the studied derivatives **6a–6g** (4.95×10^{-5} M) were obtained using a Varian Vary 100 UV-visible spectrophotometer (in

a quartz cuvette, 1 cm path length) in a 0.01 M Tris-HCl buffer (pH 7.4) at laboratory temperature. Gradually increasing concentrations of ctDNA were added to fixed concentrations of derivatives **6a–6g** [16]. Data from the spectrophotometric titrations were used for the calculation of the binding constants K for derivative-DNA complexes using the McGhee and von Hippel equation (Fig. S20) [32].

5.2.9. Fluorescence measurements

Fluorescence spectra were recorded at room temperature at a range of 500–800 nm with an excitation wavelength at 500 nm. The widths of both the excitation and emission slits were set at 10 nm. Fluorescence intensities were expressed in arbitrary units. The interactions of derivatives **6a**, **6c**, **6e** and **6g** (4.97×10^{-5} M) and **6d** and **6f** (3.98×10^{-5} M) with the ctDNA-EB complex were studied by adding specific quantities of the compound into the quartz cuvette containing a fixed concentration of the ctDNA-EB complex solution [13]. The concentration of EB was 6.0×10^{-5} M and that of the ctDNA was 1.65×10^{-5} M. The influence of the addition of each compound to the DNA-EB complex solution was observed by recording variations in the fluorescence emission spectra. All measurements were performed at 24 °C.

5.2.10. Circular dichroism

CD spectra were recorded on a Jasco J-810 spectropolarimeter in 1 mm quartz cuvettes and are the mean result of three scans from which the buffer background had been electronically subtracted. All measurements were performed in a 0.01 M Tris-HCl buffer (pH 7.4). The concentration of ctDNA was 7.66×10^{-4} M and the concentration of derivatives **6a–6g** was 8.26×10^{-6} M.

5.3. Docking studies

5.3.1. A ligand preparation

Molecular models of the Hoechst 33,258 and derivatives **6f** and **6g** were computer-built using the building options in ACD/ChemSketch [33]. The models were built as 3D structures and saved as mopcac input files using the ACD/3D Viewer [34]. MOPAC2016 was used to optimize ligand geometry [23].

5.3.2. A receptor preparation

Chimera software was used to extract the coordinates of a nucleotide from the x-ray of the Hoechst 33258/5'-d(CGCGAATTCGCG)-3' ternary complex (1d PDB: 127D). The structure of 5'-d(CGCGAATTCGCG)-3' in the canonical B-DNA helix was built using the building options included in Chimera software [25–27].

5.3.3. A charge assignment

MGL TOOLS 1.5.6 was used to assign Gasteiger partial atomic charges for ligands and for nucleotides [35]. MOPAC2016 was used to add PM7 partial atomic charges for ligands [23]. Chimera software was used to assign AMBER ff14SB partial atomic charges for the oligonucleotide [25–27].

5.3.4. The root mean square deviation calculations

Chimera software was employed to calculate RMSD [25–27].

5.3.5. Docking run

Docking simulations were carried out using Autodock ver. 4.2, while MGL TOOLS 1.5.6 was used to prepare the input files [22–27,35]. United atom representations were used for the ligand and DNA. The grid for energy for 5'-d(CGCGAATTCGCG)-3' in the canonical B-DNA helix was set at the center of macromolecule with dimensions of 80 points \times 120 points \times 80 points (x,y,z) and a spacing of 0.375 Å. The grid for energy for 5'-d(CGCGAATTCGCG)-3' (1d PDB: 127D) was set at the center of macromolecule with dimensions of 80 points \times 80

points \times 126 points (x,y,z) and a spacing of 0.375 Å.

Docking runs were performed using a Lamarckian genetic algorithm. Docking began with a population of random ligand conformations in a random orientation and at a random translation. Each docking experiment was derived from 100 different runs which were set to terminate after a maximum of 5×10^6 energy evaluations or 27×10^3 generations, yielding 100 docked conformations. The population size was set to 150. For other parameters, the default values were used.

5.4. Molecular dynamics run – A docking-like study

Molecular models of the ligand-5'-d(CGCGAATTCGCG)-3' complex for derivatives **6a**, **6d** & **6e** were prepared using the coordinates of the **6f**-5'-d(CGCGAATTCGCG)-3' complex obtained as a result of the docking simulation. Chimera software was used to rebuild ligand **6f** into ligands **6a**, **6d** & **6e** by truncating its phenylbutyl chain leaving the rest of the structure unchanged. All calculations were carried out in NAMD 2.8 using a generalized born implicit solvent for waters, parm99.dat parameters set for nucleic acids, and GAFF atom types for ligands [36–40]. ANTECHAMBER and XLEAP modules as a part of AMBERTOOLS 1.3 software package were applied to extrapolate missing ligand force-field parameters and to derive charges using AM1-BCC method.

Each complex and its components were then subjected to 3000 steps of conjugate gradient minimization followed by 6 ps MD run. Finally 3000 steps of conjugate gradient minimization were done. Energy information, averages and coordinates were recorded every 500 steps and non-bonded list was updated every 10 steps. Coordinates from MD run were employed as input data for SASAs calculations (see Chapter 5.4.1.). Final energy terms after the final minimization are shown in Table S4.

5.4.1. Calculation of solvent-accessible surface areas (SASAs)

Solvent-accessible surface areas were determined using the final coordinates from molecular dynamics simulations for free 5'-d(CGCGAATTCGCG)-3', free ligands **6a**, **6d**, **6e** & **6f** and for the ligand-5'-d(CGCGAATTCGCG)-3' complexes using Tcl module ver. 8.5.6/Tk ver. 8.5.6 of VMD 1.9.3 (Table S2, S3) [41]. Surfaces of carbon-bound hydrogens and all carbons were classified as nonpolar and those of remaining hydrophilic atoms were defined as polar for ligands. Surfaces of carbon-bound hydrogens and all carbons were classified as nonpolar and those of the remaining hydrophilic atoms were defined as polar for oligonucleotide. Surfaces were generated from coordinates with 1.4 Å surrounding radius. The change of the solvent-accessible surface area on binding, ΔA_{total} , is the difference between the area of the complex and the summed surface areas of the free DNA duplex and the free ligand:

$$A_{total} = A_{np} + A_p; \quad \Delta A_{total} = \Delta A_{np} + \Delta A_p,$$

where A_{np} and A_p represent surface contributions from nonpolar and polar atoms, respectively. The binding-induced alterations in component SASAs terms on forming the DNA-ligand complex are given by the equations:

$$\Delta A_{np} = A_{np}(\text{complex}) - [A_{np}(\text{free DNA}) + A_{np}(\text{free ligand})],$$

$$\Delta A_p = A_p(\text{complex}) - [A_p(\text{free DNA}) + A_p(\text{free ligand})].$$

Acknowledgements

This study was supported by VEGA grant No. 1/0016/18, MH CZ-DRO (UHHK, 00179906) and the State NMR Program (grant No. 2003SP200280203). Molecular graphics images were produced using UCSF Chimera package from the Resource for Biocomputing, Visualization, and Informatics at the University of California, San

Francisco (supported by NIH P41 RR-01081).

Declaration of interest

The authors have not reported any conflict of interest.

Appendix A. Supplementary data

Supplementary data to this article can be found online at <https://doi.org/10.1016/j.bioorg.2018.10.063>.

References

- [1] (a) Y. Li, X. Qi, X. Xue, X. Wu, Y. Wu, M. Chen, G. Xing, Y. Luan, J. Ren, The relationship between diphenylamine structure and NSAIDs-induced hepatocytes injury, *Toxicol. Lett.* 186 (2009) 111–114, <https://doi.org/10.1016/j.toxlet.2009.01.005>;
(b) S.M. Abou-Seri, Synthesis and biological evaluation of novel 2,4'-bis substituted diphenylamines as anticancer agents and potential epidermal growth factor receptor tyrosine kinase inhibitors, *Eur. J. Med. Chem.* 45 (2010) 4113–4121, <https://doi.org/10.1016/j.ejmech.2010.05.072>;
(c) L.S. Glass, B. Nguyen, K.D. Goodwin, C. Dardonville, W.D. Wilson, E.C. Long, M.M. Georgiadis, Crystal structure of a trypanocidal 4,4'-bis(imidazolylamino) diphenylamine bound to DNA, *Biochemistry* 48 (2009) 5943–5952, <https://doi.org/10.1021/bi900204w>.
- [2] R. Nanjunda, W.D. Wilson, Binding to the DNA minor groove by heterocyclic dications: from AT-specific monomers to GC recognition with dimers, *Curr. Protoc. Nucleic Acid Chem.* (51) (2012), <https://doi.org/10.1002/0471142700.nc0808s51Unit.8.8>.
- [3] R. Simon, S.J. Wang, Use of genomic signatures in therapeutics development, *Pharmacogenom.* J. 6 (2006) 166–173, <https://doi.org/10.1038/sj.tpj.6500349>.
- [4] G. Bischoff, S. Hoffmann, DNA-binding of drugs used in medicinal therapies, *Curr. Med. Chem.* 9 (2002) 312–348.
- [5] X. Han, X. Gao, Sequence specific recognition of ligand-DNA complexes studied by NMR, *Curr. Med. Chem.* 8 (2001) 551–581.
- [6] S. Neidle, C.M. Nunn, Crystal structures of nucleic acids and their drug complexes, *Nat. Prod. Rep.* 15 (1998) 1–15.
- [7] J. Ungvarsky, J. Plsikova, L. Janovec, J. Koval, J. Mikes, L. Mikesova, D. Harvanova, P. Fedorocko, P. Kristian, J. Kasparkova, V. Brabec, M. Vojtickova, D. Sabolova, Z. Stramova, J. Rosocha, J. Imrich, M. Kozurkova, Novel trisubstituted acridines as human telomeric quadruplex binding ligands, *Bioorg. Chem.* 57 (2014) 13–29, <https://doi.org/10.1016/j.bioorg.2014.07.010>.
- [8] C.E. Bostock-Smith, M.S. Searle, DNA minor groove recognition by bis-benzimidazole analogues of Hoechst 33258: Insights into structure-DNA affinity relationships assessed by fluorescence titration measurements, *Nucleic Acids Res.* 27 (1999) 1619–1624.
- [9] H. Ihmels, D. Otto, Intercalation of organic dye molecules into double-stranded DNA-general principles and recent developments, *Top. Curr. Chem.* 258 (2005) 161–204.
- [10] P.O. Vardevanyan, A.P. Antonyan, M.A. Parsadanyan, H.G. Davtyan, Z.R. Boyajyan, A.T. Karapetyan, Complex-formation of ethidium bromide with poly[d(A-T)]poly[d(A-T)], *J. Biomol. Struct. Dyn.* 22 (2005) 465–470, <https://doi.org/10.1080/07391102.2005.10507017>.
- [11] B.F. Cain, B.C. Baguley, W.A. Denny, Potential antitumor agents. 28. Deoxyribonucleic acid polyintercalating agents, *J. Med. Chem.* 21 (1978) 658–668.
- [12] D.J. Patel, Nuclear magnetic resonance studies of drug-nucleic acid interactions at the synthetic DNA level in solution, *Acc. Chem. Res.* 12 (1979) 118–125.
- [13] O. Salem, M. Vilková, J. Plsikova, A. Grolmusova, M. Burikova, M. Prokaiova, H. Paulikova, J. Imrich, M. Kozurkova, DNA binding, anti-tumour activity and reactivity toward cell thiols of acridin-9-ylalkenoic derivatives, *J. Chem. Sci.* 127 (2015) 931–940, <https://doi.org/10.1007/s12039-015-0851-9>.
- [14] E. Corral, A.C.G. Hotze, H. Dulk, A. Leczkowska, A. Rodger, M.J. Hannon, J. Reedijk, Ruthenium polypyridyl complexes and their modes of interaction with DNA: Is there a correlation between these interactions and the antitumor activity of the compounds? *J. Biol. Inorg. Chem.* 14 (2009) 439–448, <https://doi.org/10.1007/s00775-008-0460-x>.
- [15] J. Janočková, J. Plšiková, J. Koval, R. Jendželovský, J. Mikeš, R. Kašpárková, V. Brabec, S. Hamuláková, P. Fedoročko, M. Kožurková, Tacrine derivatives as dual topoisomerase I and II catalytic inhibitors, *Bioorg. Chem.* 59 (2015) 168–176, <https://doi.org/10.1016/j.bioorg.2015.03.002>.
- [16] I. Ahmad, A. Ahmad, M. Ahmad, Binding properties of pendimethalin herbicide to DNA: multispectroscopic and molecular docking approaches, *Chem. Phys.* 18 (2016) 6476–6485, <https://doi.org/10.1039/c5cp07351k>.
- [17] J. Janočková, E. Žilecká, J. Kašpárková, V. Brabec, O. Soukup, K. Kuca, M. Kožurková, Assessment of DNA-binding affinity of cholinesterase reactivators and electrophoretic determination of their effect on topoisomerase I and II activity, *Mol. Biosyst.* 12 (2016) 2910–2920, <https://doi.org/10.1039/C6MB00332J>.
- [18] O.M. Salem, M. Vilková, J. Janočková, R. Jendželovský, P. Fedoročko, E. Žilecká, J. Kašpárková, V. Brabec, J. Imrich, M. Kožurková, New spiro tria(thia)zolidine-acridines as topoisomerase inhibitors, DNA binders and cytostatic compounds, *Int. J. Biol. Macromol.* 86 (2016) 690–700, <https://doi.org/10.1016/j.ijbiomac.2016.02.018>.
- [19] M. Sriram, G.A. van der Marel, H.L. Roelen, J.H. van Boom, A.H. Wang, Conformation of B-DNA containing O6-ethyl-G-C base pairs stabilized by minor groove binding drugs: molecular structure of d(CGC[e6G]AATTCGCG complexed with Hoechst 33258 or Hoechst 33342, *EMBO J.* 11 (1992) 225–2327.
- [20] O. Trott, A.J. Olson, AutoDock Vina: improving the speed and accuracy of docking with a new scoring function, efficient optimization, and multithreading, *J. Comput. Chem.* 31 (2010) 455–461, <https://doi.org/10.1002/jcc.21334>.
- [21] G.M. Morris, D.S. Goodsell, R.S. Halliday, R. Huey, W.E. Hart, R.K. Belew, A.J. Olson, Automated docking using a Lamarckian genetic algorithm and empirical binding free energy function, *J. Comput. Chem.* 19 (1998) 1639–1662.
- [22] R. Huey, G.M. Morris, A.J. Olson, D.S. Goodsell, A semiempirical free energy force field with charge-based desolvation, *J. Comput. Chem.* 28 (2007) 1145–1152, <https://doi.org/10.1002/jcc.20634>.
- [23] MOPAC2016, Version: 16.146W, James J. P. Stewart, Stewart Computational Chemistry, web: <http://OpenMOPAC.net>.
- [24] J.A. Maier, C. Martinez, K. Kasavajhala, L. Wickstrom, K.E. Hauser, C. Simmerling, ff14SB: improving the accuracy of protein side chain and backbone parameters from ff99SB, *J. Chem. Theor. Comput.* 11 (2015) 3696–3713, <https://doi.org/10.1021/acs.jctc.5b00255>.
- [25] E.F. Pettersen, T.D. Goddard, C.C. Huang, G.S. Couch, D.M. Greenblatt, E.C. Meng, T.E. Ferrin, UCSF Chimera—a visualization system for exploratory research and analysis, *J. Comput. Chem.* 25 (2004) 1605–1612, <https://doi.org/10.1002/jcc.20084>.
- [26] G.S. Couch, D.K. Hendrix, T.E. Ferrin, Nucleic acid visualization with UCSF Chimera, *Nucleic Acids Res.* 34 (2006) e29, <https://doi.org/10.1093/nar/gnj031>.
- [27] Z. Yang, K. Lasker, D. Schneidman-Duhovny, B. Webb, C.C. Huang, E.F. Pettersen, T.D. Goddard, E.C. Meng, A. Sali, T.E. Ferrin, UCSF Chimera, MODELLER, and IMP: an integrated modeling system, *J. Struct. Biol.* 179 (2012) 269–278, <https://doi.org/10.1016/j.jsb.2011.09.006>.
- [28] M.T. Record Jr., J.-H. Ha, M.A. Fisher, *Methods Enzymol.* 208 (1991) 291.
- [29] J. Ren, T.C. Jenkins, J.B. Chaires, *Biochemistry* 39 (2000) 8439, <https://doi.org/10.1021/bi000474a>.
- [30] J. Carmichael, W.G. De Graff, A.F. Gazdar, J.D. Minna, J.B. Mitchell, Evaluation of a tetrazolium-based semiautomated colorimetric assay: assessment of chemosensitivity testing, *Cancer Res.* 47 (1987) 936–942.
- [31] A.R. Grivell, M.N. Berry, The effects of phosphate- and substrate-free incubation conditions on glycolysis in Ehrlich ascites tumour cells, *Biochim. Biophys. Acta* 1291 (1996) 83–88.
- [32] J.D. McGhee, P.H. von Hippel, Theoretical aspects of DNA-protein interactions: co-operative and non-co-operative binding of large ligands to a one-dimensional homogeneous lattice, *J. Mol. Biol.* 86 (1974) 469–489.
- [33] ChemSketch, ACD/Labs Release 11.00 Product version 11.02.
- [34] 3D Viewer, ACD/Labs Release 11.00 Product version 11.01.
- [35] F. Michel, M.F. Sanner, Python: a programming language for software integration and development, *J. Mol. Graph. Model.* 17 (1999) 57–61.
- [36] J.C. Phillips, R. Braun, W. Wang, J. Gumbart, E. Tajkhorshid, E. Villa, C. Chipot, R.D. Skeel, L. Kale, K. Schulten, *J. Comput. Chem.* 26 (2005) 1781–1802, <https://doi.org/10.1002/jcc.20289>.
- [37] W.L. Jorgensen, J. Chandrasekhar, J. Madura, M.L. Klein, *J. Chem. Phys.* 79 (1983) 926–935, <https://doi.org/10.1063/1.445869>.
- [38] J. Wang, P. Cieplak, P.A. Kollman, *J. Comput. Chem.* 21 (2000) 1049–1074, [https://doi.org/10.1002/1096-987X\(200009\)21:12<1049::AID-JCC3>3.0.CO;2-F](https://doi.org/10.1002/1096-987X(200009)21:12<1049::AID-JCC3>3.0.CO;2-F).
- [39] J. Wang, W. Wang, P.A. Kollman, D.A. Case, *J. Mol. Graphics Modell.* 25 (2006) 247–260, <https://doi.org/10.1016/j.jmgm.2005.12.005>.
- [40] J. Wang, R.M. Wolf, J.W. Caldwell, P.A. Kollman, D.A. Case, *J. Comput. Chem.* 25 (2004) 1157–1174, <https://doi.org/10.1002/jcc.20035>.
- [41] W.F. Humphrey, A. Dalke, K. Schulten, *J. Mol. Graphics* 14 (1996) 33–38.